G protein–coupled receptor *Gpr115* (*Adgrf4*) is required for enamel mineralization mediated by ameloblasts

Received for publication, August 3, 2020 Published, Papers in Press, August 31, 2020, DOI 10.1074/jbc.RA120.014281

Yuta Chiba[1], Keigo Yoshizaki[2], Kan Saito[1], Tomoko Ikeuchi[3], Tsutomu Iwamoto[4], Craig Rhodes[3], Takashi Nakamura[5], Susana de Vega[6], Robert J. Morell[7], Erich T. Boger[7], Daniel Martin[7], Ryoko Hino[1], Hiroyuki Inuzuka[8], Christopher K. E. Bleck[9], Aya Yamada[1], Yoshihiko Yamada[3,†,‡], and Satoshi Fukumoto[1,10,‡,*]

From the [1]Division of Pediatric Dentistry, Department of Oral Health and Development Sciences, Tohoku University Graduate School of Dentistry, Sendai, Japan, [2]Section of Orthodontics and Dentofacial Orthopedics, Division of Oral Health, Growth, and Development, Faculty of Dental Science, Kyushu University, Fukuoka, Japan, [3]Laboratory of Cell and Developmental Biology, National Institute of Dental and Craniofacial Research, National Institutes of Health, Bethesda, Maryland, USA, [4]Department of Pediatric Dentistry, Institute of Biomedical Sciences, Tokushima University Graduate School, Tokushima, Japan, [5]Division of Molecular Pharmacology and Cell Biophysics, Department of Oral Biology, Tohoku University Graduate School of Dentistry, Sendai, Japan, [6]Department of Pathophysiology for Locomotive and Neoplastic Diseases, Juntendo University Graduate School of Medicine, Tokyo, Japan, [7]Genomics and Computational Biology Core, National Institute on Deafness and Other Communication Disorders, National Institutes of Health, Bethesda, Maryland, USA, [8]Center for Advanced Stem Cell and Regenerative Research, Tohoku University Graduate School of Dentistry, Sendai, Japan, [9]Electron Microscopy Core Facility, National Heart, Lung, and Blood Institute, National Institutes of Health, Bethesda, Maryland, USA, [10]Section of Pediatric Dentistry, Division of Oral Health, Growth and Development, Faculty of Dental Science, Kyushu University, Fukuoka, Japan

Edited by Henrik G. Dohlman

Dental enamel, the hardest tissue in the human body, is derived from dental epithelial cell ameloblast-secreted enamel matrices. Enamel mineralization occurs in a strictly synchronized manner along with ameloblast maturation in association with ion transport and pH balance, and any disruption of these processes results in enamel hypomineralization. G protein–coupled receptors (GPCRs) function as transducers of external signals by activating associated G proteins and regulate cellular physiology. Tissue-specific GPCRs play important roles in organ development, although their activities in tooth development remain poorly understood. The present results show that the adhesion GPCR *Gpr115* (*Adgrf4*) is highly and preferentially expressed in mature ameloblasts and plays a crucial role during enamel mineralization. To investigate the *in vivo* function of *Gpr115*, knockout (*Gpr115*-KO) mice were created and found to develop hypomineralized enamel, with a larger acidic area because of the dysregulation of ion composition. Transcriptomic analysis also revealed that deletion of *Gpr115* disrupted pH homeostasis and ion transport processes in enamel formation. In addition, *in vitro* analyses using the dental epithelial cell line cervical loop–derived dental epithelial (CLDE) cell demonstrated that *Gpr115* is indispensable for the expression of carbonic anhydrase 6 (*Car6*), which has a critical role in enamel mineralization. Furthermore, an acidic condition induced *Car6* expression under the regulation of *Gpr115* in CLDE cells. Thus, we concluded that *Gpr115* plays an important role in enamel mineralization via regulation of *Car6* expression in ameloblasts. The present findings indicate a novel function of *Gpr115* in ectodermal organ development and clarify the molecular mechanism of enamel formation.

Dental enamel is comprised of greater than 97% hydroxyapatite and those crystals have a 1000 times greater volume as compared with that in bone or dentin, making enamel the hardest tissue in the human body (1). Dental enamel originates from dental epithelium, and tooth development is initiated by a sequential interaction of dental epithelium and mesenchyme (2). Dental epithelial stem cells invaginate into mesenchyme and form enamel organ, which is composed by mainly four distinct structures, inner enamel epithelium (IEE), outer enamel epithelium, stratum intermedium, and stellate reticulum. Ameloblasts, differentiated from IEE, are one of the most important cell types for enamel formation and their development is divided into four stages: proliferation, secretory, transition, and maturation. IEE cells, precursors of ameloblasts, exhibit high proliferation and migration activities to increase tooth germ size during the proliferation stage (3). Following the proliferation stage, IEE cells exit the cell cycle and differentiate into ameloblasts, then in the secretory stage, ameloblasts secrete enamel matrix proteins such as ameloblastin (AMBN), amelogenin, and enamelin to form an enamel scaffold (4–6). Enamel mineralization occurs subsequent to enamel matrix degradation by the activities of various proteases, such as matrix metalloproteinase-20 and kallikrein-related peptidase 4 secreted by ameloblasts in the transition stage (1, 7). Degraded enamel matrices are then absorbed by ameloblasts in the maturation stage, and mineral ion deposition takes place at the expense of scaffold enamel matrices.

Ameloblasts in the maturation stage have essential roles in ion transport for importing enamel components as well as exchange of various ions for pH regulation (8–10). In the maturation phase, ameloblasts express ion transporters or exchangers of Ca^{2+}, whereas HPO_4^{2-} promotes calcium phosphatase precipitation (8). A major biosynthesis formula for hydroxyapatite

† Deceased.
‡ These authors contributed equally to this work.
* For correspondence: Satoshi Fukumoto, fukumoto@dent.tohoku.ac.jp.

Published in the U.S.A.

($Ca_{10}(PO_4)_6(OH)_2$), synthesized from octacalcium phosphate ($Ca_8H_2(PO_4)_6{\cdot}5H_2O$), has been hypothesized (11) and is shown in the following:

$$Ca_8H_2(PO_4)_6 \cdot 5H_2O + 2Ca^{2+} \rightleftharpoons Ca_{10}(PO_4)_6(OH)_2 + 4H^+ + 3H_2O$$

This reaction occurs under a weak alkaline condition and during expansion of hydroxyapatite crystals, when protons will be released, as shown above. pH balance is strictly regulated by ameloblasts during enamel formation. A major function of the proton buffering system in ameloblasts is excretion of bicarbonates (7, 8). Ameloblasts transport bicarbonate ions through acid–base regulators, such as carbonic anhydrases (Car family), and anion exchanger 2 and bicarbonate exchangers (the solute carrier Slc4 and Slc26 families), which neutralizes protons released by mineral formation (8, 10). An effect of the ameloblast buffering system is to change enamel pH from 6.1 to 7.4 during the mineralization process (12). However, when that modulation of pH is disturbed, enamel fails to fully mineralize (11).

G protein–coupled receptors (GPCRs) consist of five main families in mammals, with more than 600 individual members known in humans (13). Tissue-specific GPCRs have essential roles in various types of organ development (14, 15), although few studies have focused on GPCRs in tooth development. In our previous study, a mouse tooth germ cDNA library was screened using DNA microarrays to identify genes preferentially expressed in tooth germs, including *Gpr115* (also known as adhesion G protein–coupled receptors subfamily F4, *Adgrf4*) (16). In addition, we have reported the biological roles of previously uncharacterized genes in tooth development (17–19). Furthermore, the functions that are characteristically expressed in tooth and affect tooth differentiation have been elucidated (20–24). In the present study, we focused on *Gpr115* as a candidate key factor for tooth development. *Gpr115* is a member of adhesion class GPCRs, the second largest GPCR subfamily, with more than 30 members (13). Although various functional contexts of adhesion class GPCRs in the immune system, neurogenesis, bone development, and cancer progression have been reported (13, 25), no findings regarding the biological function of *Gpr115* have been presented previously.

The present results indicate that *Gpr115* has an important role in tooth development. The *Gpr115*-KO mice were created to analyze its function in tooth development, and they showed enamel hypoplasia and disrupted pH buffering in enamel matrices. Additionally, *Gpr115* was found to be essential for expression of carbonic anhydrase 6 (*Car6*) in ameloblasts. Results of *in vitro* experiments with the mouse dental epithelial cell line CLDE revealed that both *Gpr115* and *Car6* are essential for mineralization activity. Furthermore, we analyzed the gene expression of CLDE cells and found that the expression of *Car6* was up-regulated under an acidic condition via *Gpr115* expression. Together, *Gpr115* was shown to function as a regulator of *Car6* expression to buffer protons produced by hydroxyapatite growth during enamel mineralization.

Results

Gpr115 was highly expressed during tooth development and localized in developing ameloblasts

Initially, the expression of Gpr115 during tooth development was analyzed. Both Northern blotting (Fig. 1*A*) and RT-qPCR (Fig. 1*B*) results of postnatal day (P) 1 mice showed a high level of Gpr115 expression in teeth. Furthermore, RT-PCR analysis of P1, P3, P7, and P12 mouse molars (Fig. 1*C*) showed that Gpr115 expression was increased sequentially during tooth development. In P3 molars, Gpr115 expression was observed in both dental epithelium and mesenchyme, although higher in dental epithelium (Fig. 1*D*). *In situ* hybridization in P1 mouse molars to detect the transcript of Gpr115 in tooth germ sections (Fig. 1*E*) revealed that Gpr115 was localized in ameloblasts and odontoblasts. Further immunostaining of P7 molars and P15 incisors also showed Gpr115 specifically expressed in ameloblasts and odontoblasts (Fig. 1, *F* and *G*).

Gpr115-KO mice showed hypomineralization, dysregulation of element composition, larger acidic area in enamel

Next, *Gpr115* knockout (*Gpr115*-KO) mice were created to determine the *in vivo* function of *Gpr115* during tooth development (Fig. 2*A*). The loxP sites in floxed alleles were recombined by mating with CMV-Cre mice to delete exon 4 of *Gpr115* from the entire body. The *Gpr115*-KO mouse genotype was analyzed using genomic PCR (Fig. 2*B*), with deletion of *Gpr115* mRNA validated by RT-qPCR analysis of P7 WT and *Gpr115*-KO molars (Fig. 2*C*). Deletion of exon 4 caused a frameshift mutation and resulted in a short GPR115 protein (Fig. 2, *D* and *E*). As a result, immunostaining analysis using an anti-GPR115 C terminus antibody did not detect the GPR115 protein in ameloblasts or odontoblasts of P7 *Gpr115*-KO molars (Fig. 2*F*).

Gpr115-KO mice were viable and fertile, although the enamel surface of mandibular incisors at the age of 8 weeks had a chalky white color, a characteristic of enamel hypoplasia (Fig. 3*A*, *b* and *d*). Maxillary incisors extracted from *Gpr115*-KO mice showed a smaller yellow-colored area, indicating that the tooth abnormality existed in the enamel surface (Fig. 3*Af*). However, histological analysis of P7 molars and P15 incisors of *Gpr115*-KO mice did not reveal apparent ameloblast-related morphological differences (Fig. 3, *B* and *C*). We then performed micro-CT analyses of whole mandibles obtained from 8-week-old WT and *Gpr115*-KO mice (Fig. 4), and 3D images reconstructed from micro-CT scanning showed decreased incisor enamel length in the *Gpr115*-KO mandibles (Fig. 4*Ad*). The volume of enamel in incisors of *Gpr115*-KO was ~17% less and 15% less in molars as compared with those in WT mice (Fig. 4*B*). We also determined the mineral density of enamel at different levels of incisor development (Fig. 4*C*): protected late maturation enamel (*position 1*), early maturation of enamel (*position 2*), and transition to maturation of enamel (*position 3*). At the level of early maturation of enamel (*position 2*), which is the section in the center of the first molar, the density of enamel in *Gpr115*-KO mice incisor was significantly lower as compared with the WT samples (Fig. 4*D*). These results indicate that deletion of *Gpr115* results in hypomineralized enamel formation.

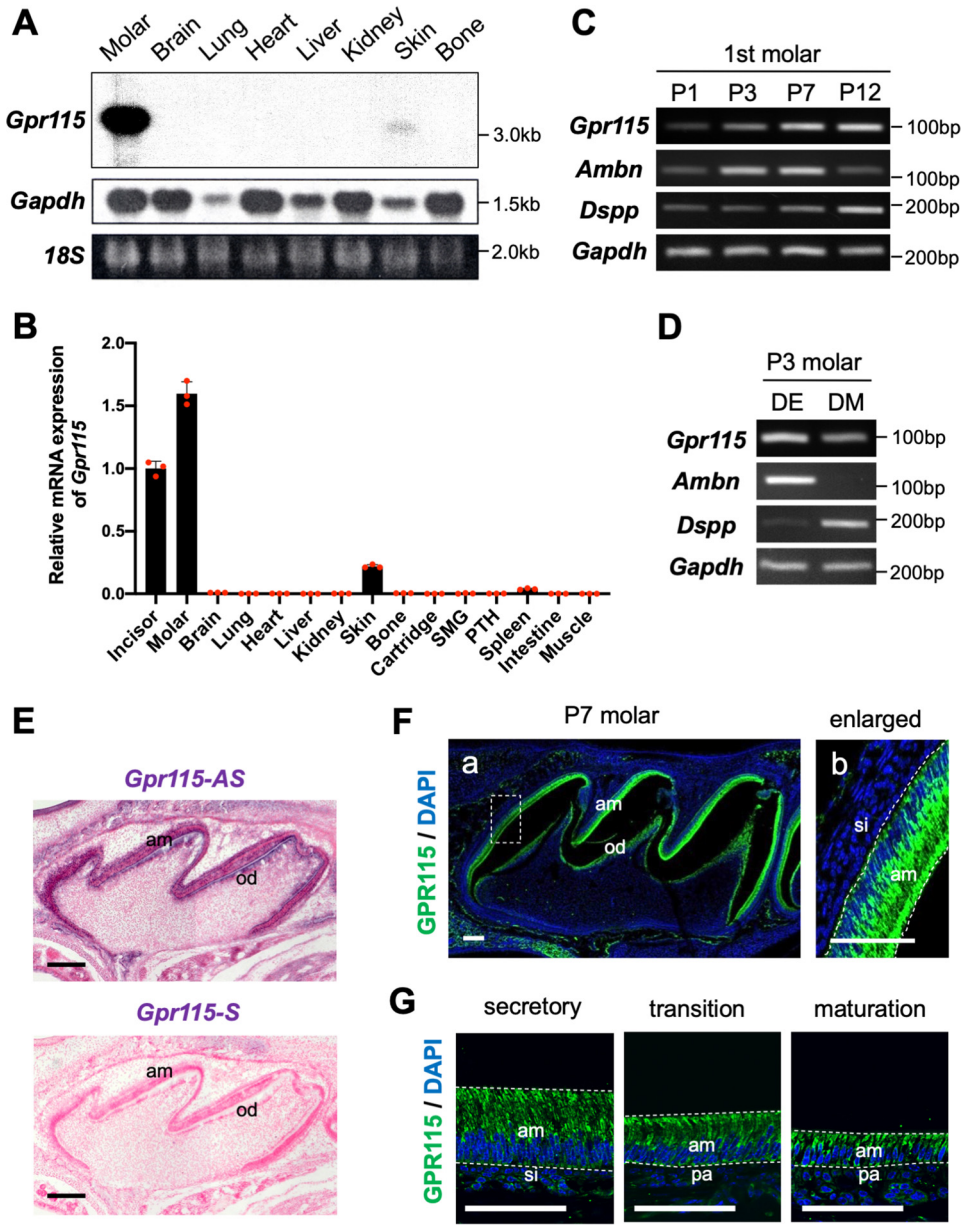

Figure 1. *Gpr115* expression in developing tooth germ. *A*, *Gpr115* mRNA expression in different tissues obtained from P1 mice were analyzed by Northern blotting. *Gapdh* and *18S* were used as internal controls. *B*, *Gpr115* mRNA expression in different tissues obtained from P1 mice was analyzed by RT-qPCR. *Gpr115* expression was normalized to that of *Gapdh* ($n = 3$). Mean values are shown as *bars*. *Error bars* represent S.D. *C*, RT-PCR analysis of *Gpr115*, *Ambn*, and *Dspp* expressions in P1, P3, P7, and P12 mouse molars. *Gapdh* was used as an internal control. Three independent experiments were performed. *D*, RT-PCR analysis of *Gpr115*, *Ambn*, and *Dspp* expressions in P3 mouse molar epithelium and mesenchyme. *Gapdh* was used as an internal control. *DE*, dental epithelium; *DM*, dental mesenchyme. *E*, *In situ* hybridization of *Gpr115* in P1 mouse molars. *AS*, antisense probe; *S*, sense probe. *Purple*, *Gpr115*. *Scale bars*, 100 μM. *F*, *a*, immunofluorescence of GPR115 in P7 molar. *b*, enlargement of *a*. *G*, immunofluorescence of GPR115 in P15 incisor. *First column*, secretory stage; *second column*, transition stage; *third column*, maturation stage. *Green*, GPR115; *blue*, DAPI. *am*, ameloblast; *si*, stratum intermedium; *od*, odontoblast; *pa*, papillary layer. *Dashed lines* indicate ameloblast border. *Scale bars*, 100 μM.

The detailed structure of incisor enamel was further analyzed using scanning EM (SEM) (Fig. 5*A*). In an incisor section of *Gpr115*-KO mice, lingual enamel shows a porous structure and a part of enamel rod, a crystal unit of enamel hydroxyapatite was not formed (Fig. 5*Ad*). In WT incisor lingual enamel, the outer enamel surface layer exists adjacent to the aprismatic enamel layer (Fig. 5*Ae*). Although in the *Gpr115*-KO incisor lingual enamel, the outer enamel surface was absent (Fig. 5*Af*), SEM–energy-dispersive X-ray spectroscopy (EDX) analysis of *Gpr115*-KO enamel showed an abnormal composition of elements, including decreased carbon, increased oxygen, and phosphate and calcium (Fig. 5*B*). A pH indicator staining method was used to determine enamel acidity in incisors from 8-week-old WT and *Gpr115*-KO mice (Fig. 5*C*). Using colorimetric indicators, it was shown that the secretory areas of enamel had an acidic condition, whereas maturated enamel had an alkalic condition (26). Bromphenol red staining shows a pH value of ~6.5–7.0 as light purple, whereas a value close to 7.5 has no staining (26). The longer area of maturated enamel in *Gpr115*-KO incisors was stained a red purple color than that

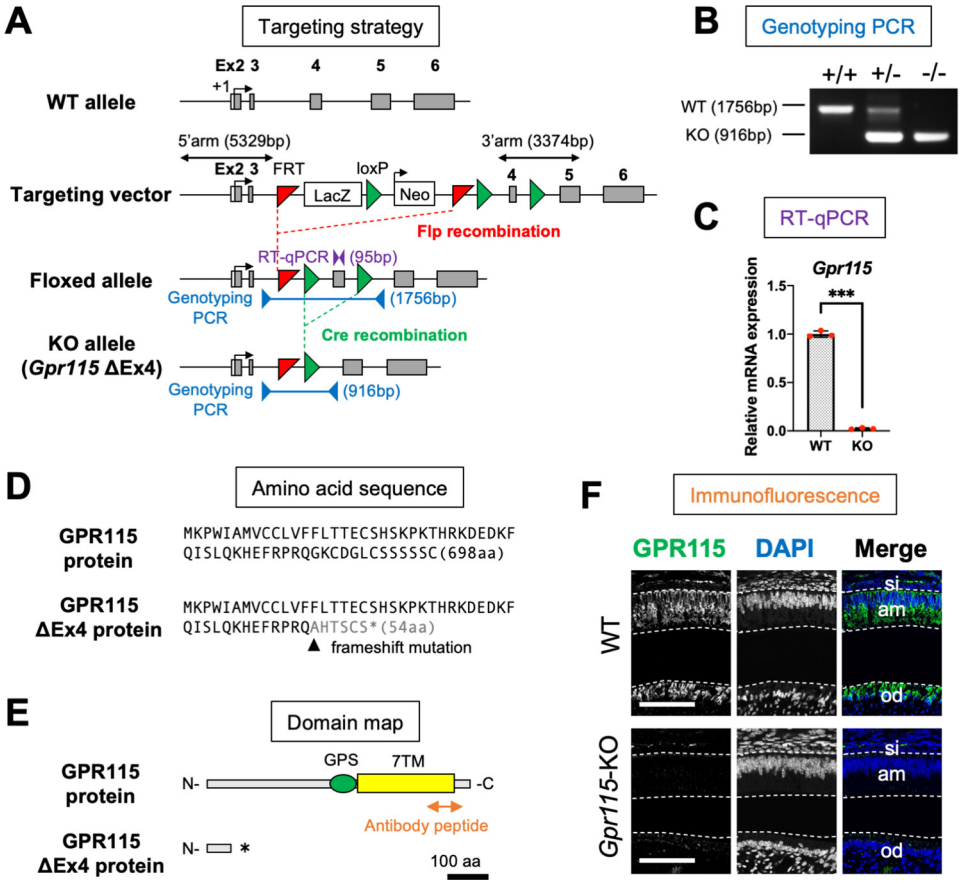

Figure 2. Generation of *Gpr115*-KO mice. *A*, schematic diagram of WT allele of Gpr115 gene, targeting vector, floxed allele after homologous recombination, and KO allele after Cre recombination. The 5′ and 3′ arms were designed for homologous recombination. The neomycin-resistance gene was driven by the human β-actin promoter. FRT sites were removed by Flp recombination in the floxed allele. *Gpr115* exon (*Ex*) 4 was deleted by CMV promoter–driven Cre recombination. *Arrows* indicate primer used for genotyping. *Arrow* indicates transcription start site. *Purple arrowheads* indicate primer used for RT-qPCR for detecting cDNA of exon 4. *Blue arrowheads* and *lines* indicate primers used for genotyping and PCR products, respectively. *B*, genomic PCR of $Gpr115^{+/+}$ (WT), $Gpr115^{+/-}$ (heterozygous), and $Gpr115^{-/-}$ (KO). The PCR product of the KO allele was smaller than that of the WT allele. *C*, mRNA expression of *Gpr115* in WT and *Gpr115*-KO P7 molars. *Gpr115* expression was normalized to that of *Gapdh* ($n = 3$). Mean values are shown as *bars*. *Error bars* represent S.D. ***, $p < 0.001$; two-tailed *t* test. Three independent experiments were performed. *D*, the first 60 amino acid (aa) sequences of the WT and *Gpr115*-KO products are shown. In *Gpr115*-KO mice, the frameshift caused an early termination codon, resulting in a short protein consisting of 54 aa. *Asterisk* indicates termination codon. *E*, domain structure of GPR115 predicted by PROSITE. *Scale bar*, 100 aa. *Asterisk* indicates termination codon. *Arrow* indicates location of anti-GPR115 antibody immunogen peptide. *F*, immunofluorescence of *Gpr115* in WT and *Gpr115*-KO P7 molars. *Green*, *Gpr115*; *blue*, DAPI. *am*, ameloblast; *si*, stratum intermedium; *od*, odontoblast. *Dashed lines* indicate ameloblast border and odontoblast order. *Scale bars*, 50 μm. *Blue arrows* indicate primer used for genotyping. *Black arrow* indicates transcription start site.

of WT, indicating an acidic condition (Fig. 5*C*, *left panel*). Furthermore, both bromphenol red and resazurin staining showed that the acidic area of incisor enamel in *Gpr115*-KO was larger than that in WT mice (Fig. 5*C*). These results suggested that ion transport related to enamel formation may be disturbed in *Gpr115*-KO mice.

Deletion of Gpr115 did not alter the expression of major enamel matrix proteins or proteases

Gpr115-KO mice showed a hypomineralization type of enamel hypoplasia (1). To identify the molecular mechanism of abnormal enamel formation in those mice, RNA-Seq analysis was performed with P7 molars from WT and *Gpr115*-KO mice. Complete absence of exon 4 in the *Gpr115*-KO samples was confirmed by visualization of RNA-Seq coverage data (Fig. 6*A*). Additionally, differential expression analyses of WT and *Gpr115*-KO samples revealed that the expressions of enamel matrix genes *Ambn*, *Enam*, and *Amtn* and protease genes *Mmp-20*, *Klk4*, and alkaline phosphatase (*Alpl*) were not affected by deletion of *Gpr115* (Fig. 6*B*). RT-qPCR results also demonstrated unaltered mRNA expression of those genes (Fig. 6*C*), whereas immunostaining analysis revealed that protein expression of AMBN was not suppressed in P7 *Gpr115*-KO molars (Fig. 6*D*). These results indicated that the enamel matrix protein and protease expressions were not affected by deletion of *Gpr115*.

Deletion of Gpr115 down-regulated expression of carbonic anhydrase 6 in ameloblasts

Gene ontology (GO) enrichment analysis of differentially expressed genes in P7 WT and *Gpr115*-KO molars was performed using RNA-Seq data to categorize genes in which expression was affected by deletion of *Gpr115* (Fig. 7*A*). The GO terms for ion homeostasis and transport are highly enriched, indicating that *Gpr115* is essential for regulation of ion homeostasis and transport during ameloblast development.

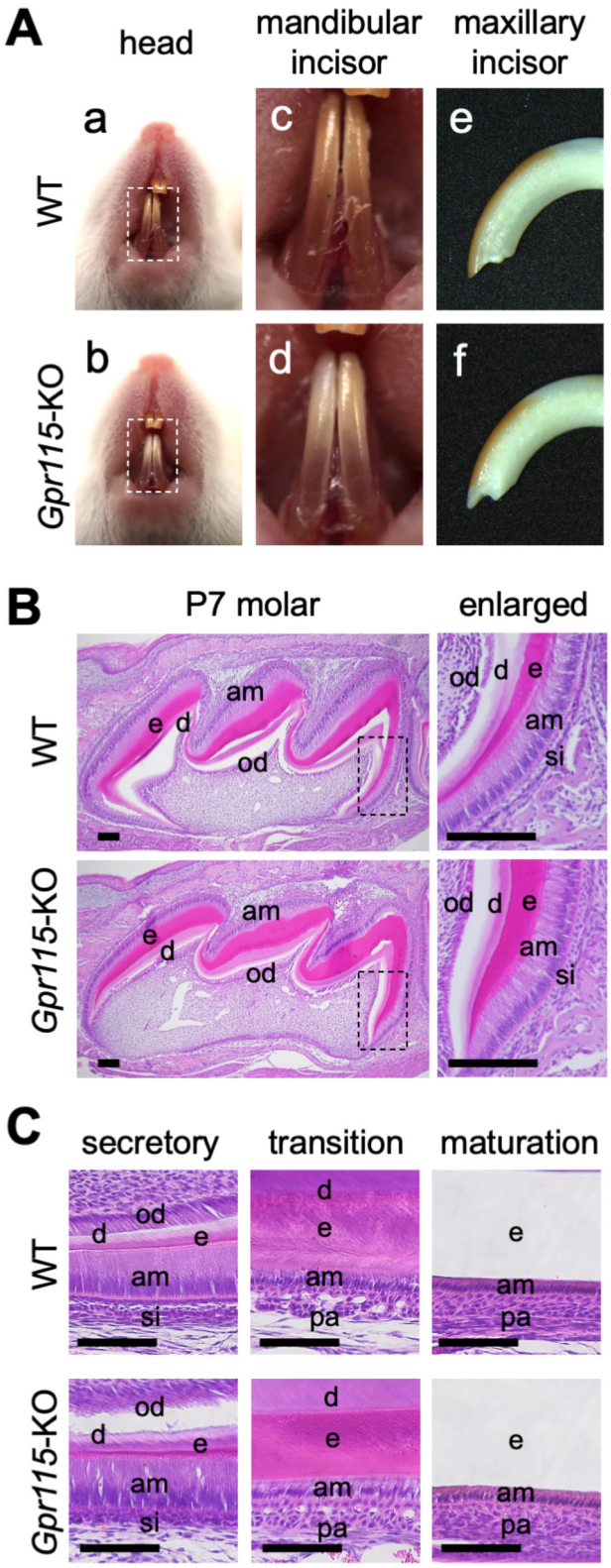

Figure 3. Chalky white colored incisors from *Gpr115*-KO mice. *A*, photographic analyses of 8-week-old WT and *Gpr115*-KO incisors. *Second column* shows enlargement of *first column*. *Third column*, maxillary incisors. *B*, H&E staining of molars from P7 WT (*upper panel*) and *Gpr115*-KO (*lower panel*) mice. *Second column*, enlargement of data shown in *first column*. *Dashed lines* indicate enlarged area. *C*, H&E staining of P15 WT (*upper panel*) and *Gpr115*-KO (*lower panel*) incisors. *First column*, secretory stage. *Second column*, transition stage. *Third column*, maturation stage. *am*, ameloblast; *si*, stratum intermedium; *od*, odontoblast; *e*, enamel; *d*, dentin; *pa*, papillary layer. *Scale bars*, 100 μM.

Scatter plot analysis of RNA-Seq data showed a high level of expression of the ion exchanger carbonic anhydrase 6 (*Car6*) in WT mice as compared with *Gpr115*-KO molars (Fig. 7*B*). The gene expressions of ion transporters and carbonic anhydrase family members, which have been reported to play important roles in tooth development (8), were examined. We evaluated ion transporters and carbonic anhydrases gene expression level in our WT and *Gpr115*-KO dataset. Heat map analysis indicated that expressions of major ion transporter genes (Fig. 7*C*) and carbonic anhydrases (Fig. 7*D*) expressed in ameloblasts were not altered, except for that of *Car6*. RT-qPCR results of P7 WT and *Gpr115*-KO molars also revealed depletion of *Car6* expression in *Gpr115*-KO (Fig. 7*E*). Immunostaining of CAR6 in P7 WT and *Gpr115*-KO molars was subsequently done to examine the protein expression of *Car6* (Fig. 7*F*). In WT molars, *Car6* expression was noted in ameloblasts and odontoblasts in WT mice (Fig. 7*F, a* and *c*), whereas its expression was suppressed in *Gpr115*-KO molars (Fig. 7*F, b* and *d*), suggesting that *Gpr115* is essential for expression of *Car6 in vivo*.

Next, CLDE, a mouse-derived dental epithelial cell line, was used to analyze the effect of *Gpr115* on *Car6* expression (Fig. 8*A*). *Gpr115*-knockdown CLDE cells using siRNA of *Gpr115* down-regulated the expression of *Car6* (Fig. 8*A*) at 72 h after transfection, indicating that *Gpr115* regulates *Car6* expression during tooth development. However, knockdown of *Car6* expression in CLDE cells using siRNA of *Car6* did not have effects on *Gpr115* expression (Fig. 8*B*). The effect of Gpr115 on mineralization activity in dental epithelial cells was also examined using Alizarin Red staining (Fig. 8, *C* and *D*). Using CLDE cells cultured in mineralization conditioned medium for 2 or 4 weeks, mineralization activity was significantly inhibited in *Gpr115*-knockdown CLDE cells as well as *Car6*-knockdown CLDE cells (Fig. 8*D*), suggesting that both Gpr115 and Car6 are essential for enamel mineralization. Furthermore, whether overexpression of Car6 rescues loss of mineralization activity caused by depletion of Gpr115 or Car6 in CLDE cells was also examined (Fig. 8, *E* and *F*). As expected, Car6 overexpression promoted mineralization activity in *Gpr115*-knockdown as well as *Car6*-knockdown CLDE cells (Fig. 8*F*).

pH decline induced expression of Car6 via Gpr115 in dental epithelial cell line

Carbonic anhydrases catalyze the interconversion between carbon dioxide and water and bicarbonate. During enamel formation, hydroxyapatite crystals produce protons and induce crystal size growth (7). These hydroxyapatite crystals could be unstable under pH 5.5 (12). For this reason, pH cycling during enamel formation is modulated between 6.1 and 7.4 by the proton buffering system. The bicarbonate buffer system has important role to neutralize protons produced from enamel, thus carbonic anhydrases contribute to enamel formation (8, 10). We examined the effects of pH changes on gene expression in dental epithelium using differentially pH-adjusted culture medium for CLDE cells (Fig. 9*A*). RT-qPCR results revealed that pH decline induced expressions of *Gpr115* and *Car6* in CLDE cells, suggesting that an acidic condition promotes their expression in ameloblasts. Furthermore, the effect of *Gpr115*

ASBMB

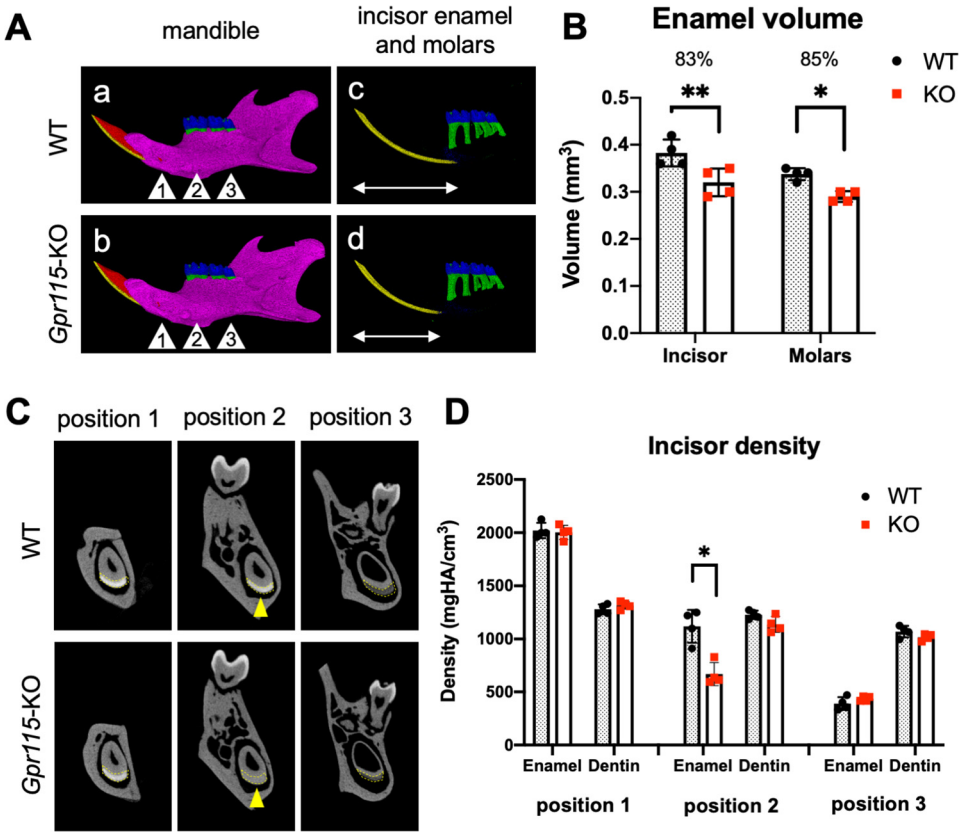

Figure 4. Defective enamel mineralization in *Gpr115*-KO mice. *A*, micro-CT analyses of 8-week-old WT and *Gpr115*-KO mandibles. *First column* (*a* and *b*), 3D reconstructed image of mandible. *Second column* (*c* and *d*), 3D reconstructed image of molars and incisor enamel. *c* and *d* correspond to *a* and *b*, respectively. *Blue*, molar enamel; *yellow*, incisor enamel. *Arrows* indicate position used for measurement of enamel mineral density in *C*. *B*, total volumes of enamel in 8-week-old WT and *Gpr115*-KO molars and incisors ($n = 4$). Number above *bar graph* indicates ratio of volume (KO/WT). Mean values are shown as *bars*. *Error bars* represent S.D. **, $p < 0.01$; two-tailed *t* test. *C*, cross sections of micro-CT analysis images of WT and *Gpr115*-KO incisors. *Position 1*, late maturation of enamel; *position 2*, early maturation of enamel; *position 3*, transition stage of enamel. *Dashed lines* indicate enamel area. *Arrowheads* indicate differences in enamel density between cross sections of incisors from WT and *Gpr115*-KO mice. *D*, quantification of enamel and dentin mineral density. Cross sections in *C* indicate positions of measurement ($n = 4$). Mean values are shown as *bars*. *Error bars* represent S.D. *, $p < 0.05$; two-tailed *t* test.

knockdown to *Car6* mRNA induction under high (pH 7.8) or low (pH 5.8) pH condition was examined in CLDE cells (Fig. 9*B*). The level of *Car6* expression was similar in *Gpr115* knockdown and control cells cultured in pH 7.8 media, because of the low expression level of Car6 in CLDE cells at that pH. *Car6* expression level is suppressed in *Gpr115* knockdown cells cultured with pH5.8 media compared with control. These results suggested that an acidic condition promotes expression of *Car6* via induction of *Gpr115* expression.

Discussion

The present study examined the role of *Gpr115* in tooth development. Its expression was noted in ameloblasts and odontoblasts (Fig. 1, *E* and *F*) and shown to contribute to the enamel mineralization process via regulation of *Car6* expression. In molars obtained from *Gpr115*-KO mice, *Car6* expression was suppressed in ameloblasts (Fig. 7), indicating that pH homeostasis was disturbed. Furthermore, incisors in those mice had a chalky white appearance, a typical phenotype demonstrating hypomaturation of enamel hypoplasia. The color change in the enamel surface corresponded to SEM results showing that the outer enamel surface was deficient in *Gpr115*-KO incisors (Fig. 5*A*). The outer enamel surface is formed at the end of enamel formation and greater amounts of inorganic ions, such as ferritin ion, are contained in the outer layer to help resisting various stimuli in the oral cavity (27). The abnormality of ion composition observed in *Gpr115*-KO enamel (Fig. 5*B*) suggests that ion transport in ameloblasts was disturbed by *Gpr115* deletion. Additionally, we observed a porous dentin structure in *Gpr115*-KO incisors using SEM analysis (data not shown). Thus, Gpr115 may also have a role in dentin development processes.

Car6 expression was also found to be suppressed in *Gpr115*-KO molars (Fig. 7, *E* and *F*) as well as *Gpr115*-knockdown CLDE cells (Fig. 8*A*). *Car6* is expressed in mature ameloblasts, and catalyzes the interconversion between protons and bicarbonate ions into carbon dioxide and water, and functions as an acid–base regulator. Because of low Car6 expression level in *Gpr115*-KO mice, ameloblasts do not neutralize protons produced during the process of enamel crystal formation. Our findings indicated that enamel mineralization was disturbed under an acidic condition, which resulted in a lack of outer enamel surface and lower mineral density in formed enamel. We examined the effects of Gpr115 and Car6 on mineralization activity of CLDE cells using Alizarin Red staining (Fig. 8, *C–F*). Both *Gpr115*-knockdown and *Car6*-knockdown CLDE cells showed lower levels of mineralization activity than the mock

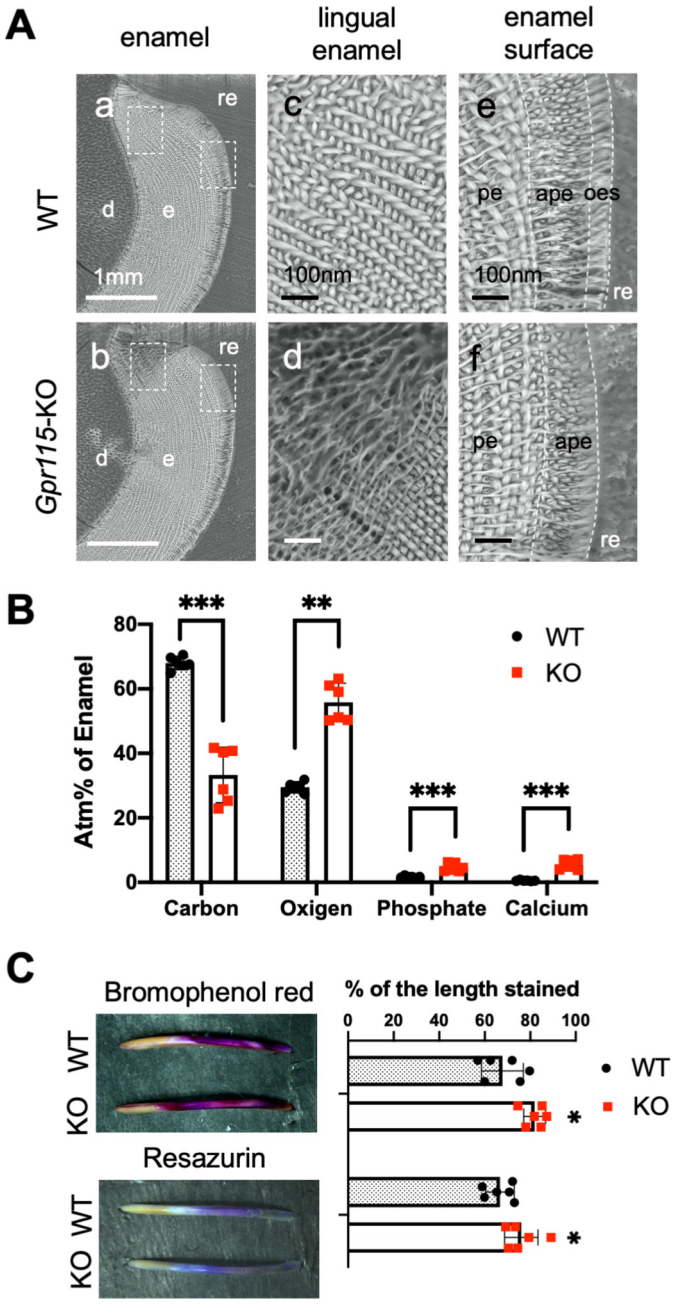

Figure 5. Dysregulation of ion composition and pH in *Gpr115*-KO enamel. *A*, scanning EM images of sections from 8-week-old WT and *Gpr115*-KO incisors. *a* and *b*, incisor sections are shown. *Dashed boxes* are areas shown in *c–f*. *Scale bars*, 1 mm. *re*, resin; *e*, enamel; *d*, dentin. *c* and *d*, high magnification of lingual enamel. *e* and *f*, high magnification of enamel surface. *Dashed lines* indicate border of aprismatic enamel and outer enamel surface. *re*, resin; *pe*, prismatic enamel; *ape*, aprismatic enamel; *oes*, outer enamel surface. *Scale bars*, 100 nm. *B*, ion composition in WT and *Gpr115*-KO enamel determined by SEM-EDX analysis ($n = 6$). Mean values are shown as *bars*. *Error bars* represent S.D. **, $p < 0.01$; ***, $p < 0.001$; two-tailed *t* test. *C*, staining of 8-week-old WT and *Gpr115*-KO incisors to indicate pH. *Left column*, bromphenol red and resazurin staining of WT and *Gpr115*-KO incisors. *Right column*, quantified data showing stained incisor length by pH indicators ($n = 6$). *Upper right*, bromphenol red staining, *lower right*, resazurin staining. Mean values are shown as *bars*. *Error bars* represent S.D. *, $p < 0.05$; two-tailed *t* test.

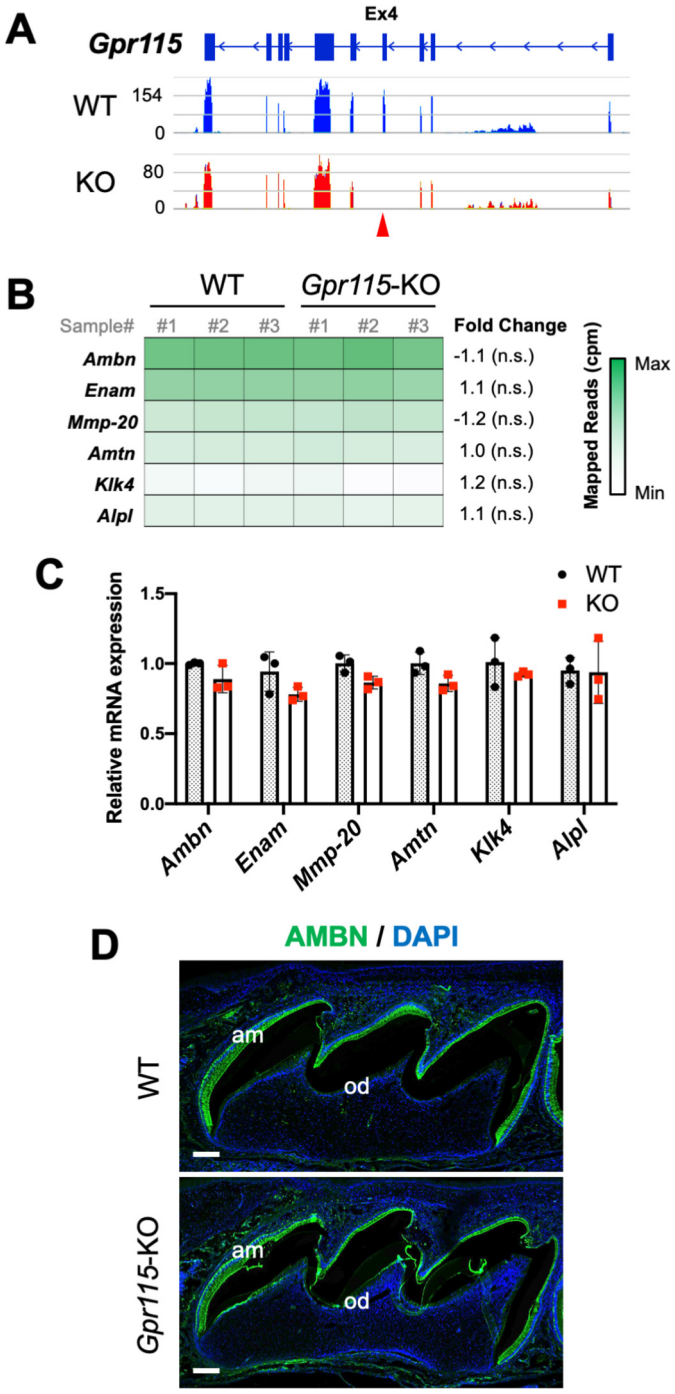

Figure 6. Unaltered expressions of enamel matrix proteins and proteases in *Gpr115*-KO teeth. *A*, visualization of RNA-Seq coverage data for *Gpr115* locus from P7 WT and *Gpr115*-KO molars. *y* axis represents mapped reads. *Arrowhead* indicates deleted *Gpr115* exon 4 (*Ex4*). *B*, heat map of enamel matrix protein and protease expressions generated from RNA-Seq analysis of P7 WT and *Gpr115*-KO molars. *C*, mRNA expressions of enamel matrix proteins and proteases were validated by RT-qPCR in P7 WT and *Gpr115*-KO molars ($n = 3$). *Error bars* represent S.D.; *n.s.*, $p > 0.05$; two-tailed *t* test. Three independent experiments were performed. *D*, immunofluorescence of AMBN in molars from WT and *Gpr115*-KO P7 mice. *Green*, AMBN; *blue*, DAPI. *am*, ameloblast; *od*, odontoblast. *Scale bars*, 100 μM.

control cells (Fig. 8, *C* and *D*). Interestingly, overexpression of Car6 partially rescued mineralization activity in both of those knockdown cell lines (Fig. 8, *E* and *F*). These results indicate that suppression of Car6 expression may be the main cause of inhibition of mineralization in CLDE cells.

Previous reports have noted expressions of several carbonic anhydrases in ameloblasts and carbonic anhydrase family

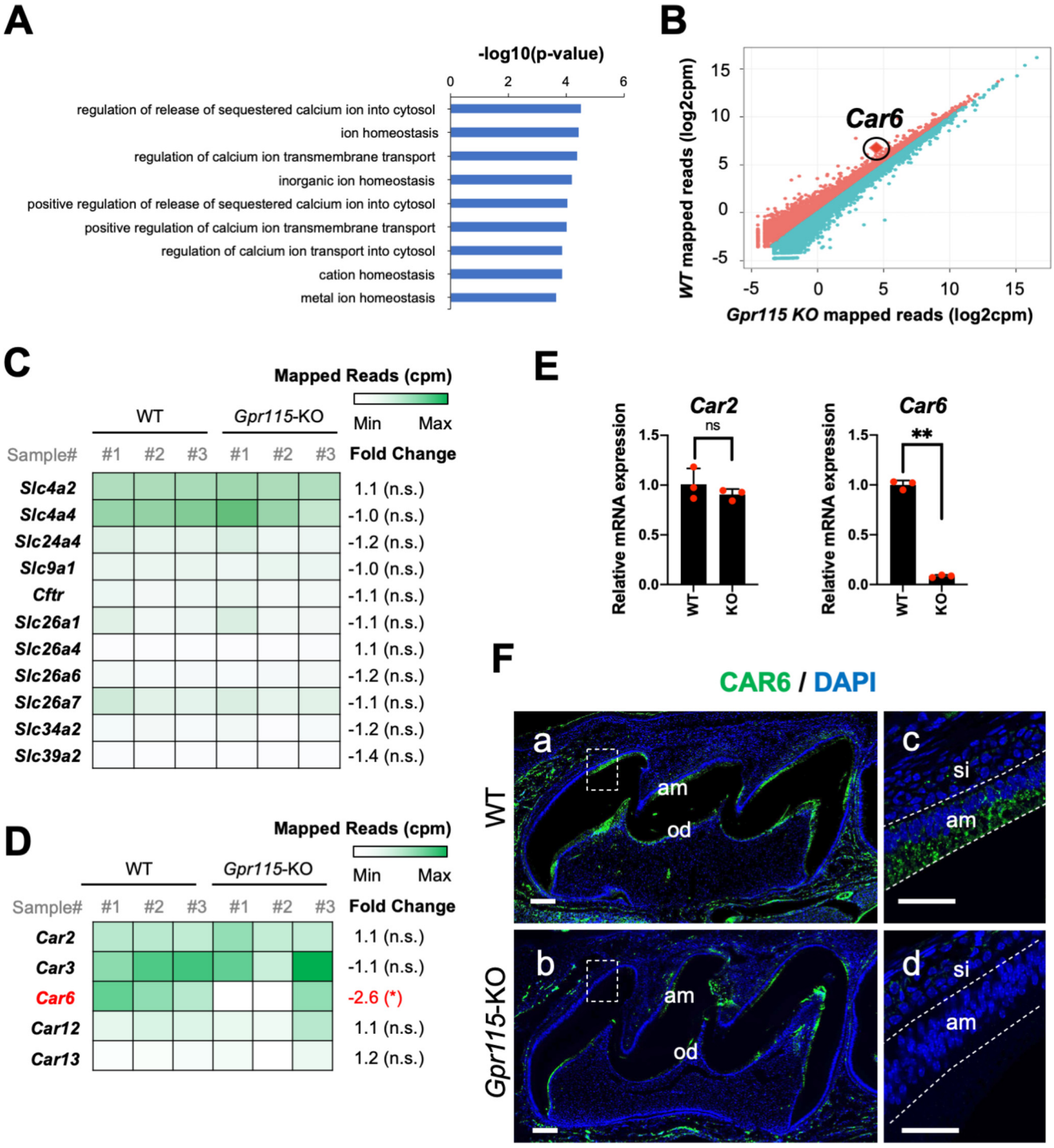

Figure 7. Deletion of Gpr115 suppressed expression of Car6 during tooth development. *A*, GO analysis of different expressions in P7 WT and *Gpr115*-KO molars. *B*, scatter plot analysis obtained by RNA-Seq showing genes differently expressed in P7 WT and *Gpr115*-KO molars. *Highlighted plot*, *Car6*. *Red and blue plots*, up- and down-regulated genes, respectively. *C*, heat map of ion transporters expressed in P7 WT and *Gpr115*-KO molars generated from RNA-Seq analysis. *D*, heat map of carbonic anhydrase family expressed in P7 WT and *Gpr115*-KO molars generated from RNA-Seq analysis. *E*, mRNA expressions of *Car2* and *Car6* were validated by RT-qPCR in P7 WT and *Gpr115*-KO molars ($n = 3$). *Error bars* represent S.D.; *ns*, $p > 0.05$, **, $p < 0.01$; two-tailed *t* test. Three independent experiments were performed. *F*, CAR6 immunofluorescence in WT and *Gpr115*-KO P7 molars. *c* and *d*, enlargement of *a* and *b*. *Green*, CAR6; *blue*, DAPI. *am*, ameloblast; *si*, stratum intermedium; *od*, odontoblast. *Scale bars*, 100 μM.

members have been suggested to play a role in enamel mineralization (28–31). Interestingly, in the present study, deletion of *Gpr115* did not alter in the expression of carbonic anhydrase family in molars, except for *Car6* (Fig. 7*D*). *Car6* is a secretory type of carbonic anhydrase and may have different roles as compared with other carbonic anhydrases in enamel formation, as well as a different gene regulation mechanism. The homeodomain transcription factor Dlx3 has been shown to bind to the *Car6* and *Car2* promoter regions to regulate *Car6* but not *Car2* expression, in developing rat incisor enamel

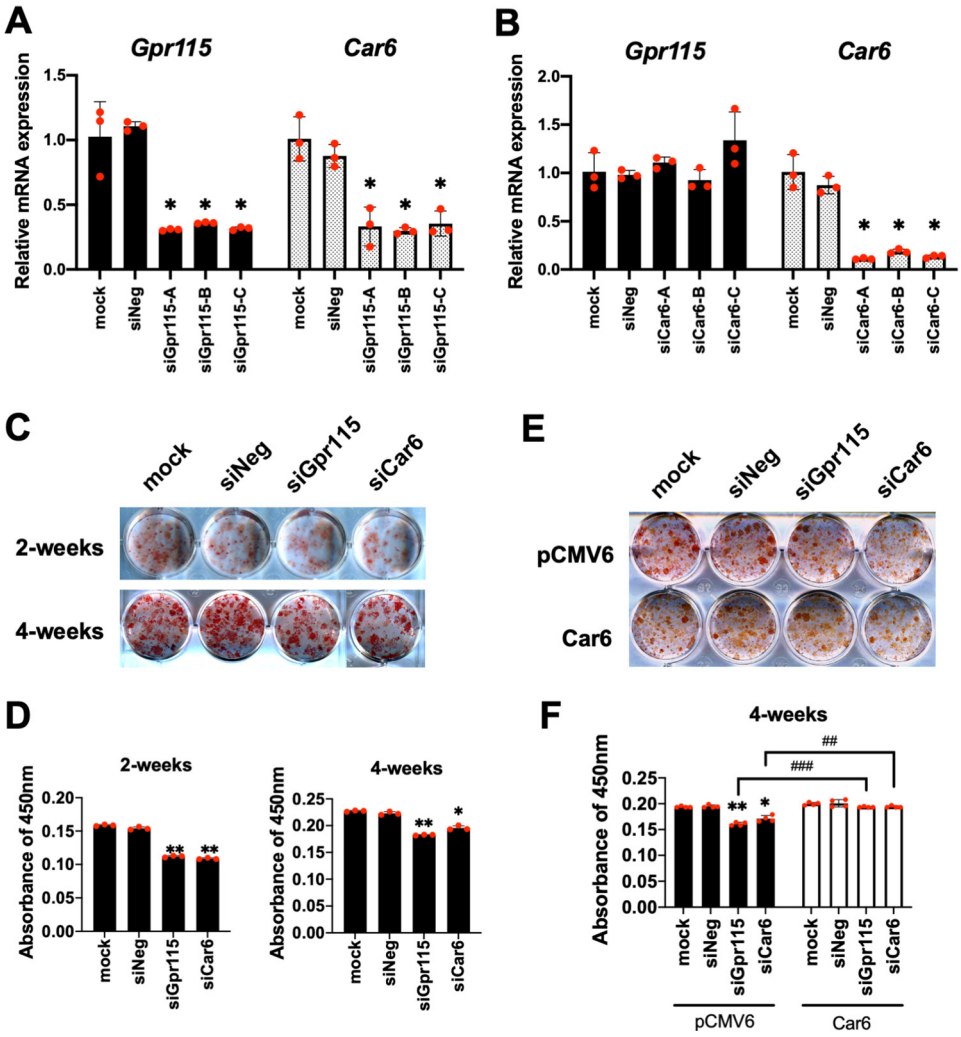

Figure 8. Gpr115 knockdown suppressed cellular mineralization activity of dental epithelial cell line CLDE. *A*, mRNA expression of *Gpr115* and *Car6* determined in control mock without siRNA (*mock*), negative control siRNA (*siNeg*), and siGpr115-transfected CLDE cells ($n = 3$). *Error bars* represent S.D.; *, $p < 0.05$; two-tailed *t* test as compared with mock sample. Three independent experiments were performed. *B*, mRNA expressions of *Gpr115* and *Car6* determined in control mock without siRNA (*mock*), negative control siRNA (*siNeg*), and siCar6-transfected CLDE cells ($n = 3$). *Error bars* represent S.D.; *, $p < 0.05$; two-tailed *t* test as compared with mock sample. Three independent experiments were performed. *C*, mineralization activity assessed by Alizarin Red staining in control without siRNA (*mock*), and siNeg-, siGpr115-, and siCar6-transfected CLDE cells after 2 and 4 weeks of culture. *D*, Alizarin Red staining was performed by dissolving with 1% SDS and absorbance at 450 nm was measured at 2 (*left panel*) and 4 weeks (*right panel*) ($n = 3$). Mean values are shown as *bars*. *Error bars* represent S.D.; *, $p < 0.05$; **, $p < 0.01$; two-tailed *t* test. Three independent experiments were performed. *E*, mineralization activity was assessed by Alizarin Red staining in mock as well as siNeg-, siGpr115-, and siCar6-transfected CLDE cells with pCMV6- or Car6-overexpression after 4 weeks of culture. *F*, Alizarin Red staining was performed by dissolving with 1% SDS, then absorbance at 450 nm was determined after 4 weeks ($n = 4$). Mean values are shown as *bars*. *Error bars* represent S.D.; *, $p < 0.05$, **, $p < 0.01$ as compared with mock with pCMV6-overexpressed CLDE cells; two-tailed *t* test. ##, $p < 0.01$; ###, $p < 0.001$ as compared with siGpr115 or siCar6 with Car6-overexpressed CLDE cells; two-tailed *t* test. Four independent experiments were performed.

organs (31). Furthermore, those authors reported that epithelial cell–specific K14-promoter–dependent conditional knockout of Dlx3 resulted in a hypomaturation type of enamel hypoplasia, similar to that seen in the present *Gpr115*-KO mice. These findings indicate an indispensable role for *Car6* in enamel maturation. We attempted to examine the relationship between Car6 transcription and Gpr115 by knockdown of Dlx3 in CLDE cells, although that knockdown did not have a significant effect on Car6 expression in this cell line (data not shown). Additional analysis will be needed to reveal the molecular mechanism related to transcriptional regulation of Car6.

During the maturation stage of enamel development, pH changes occur, termed pH cycling. In this step, ameloblasts transform their morphology from ruffle-ended to smooth-ended (7, 10). These ameloblast phases correspond to the pH of enamel, although the detailed mechanism has yet to be clarified (7). In the present study, the affection of different pH on CLDE cell experiment showed that expressions of *Gpr115* and *Car6* were induced under an acidic condition (Fig. 9), indicating that ameloblasts may respond to protons released by enamel mineralization and induce *Gpr115* and *Car6* expression to buffer those protons. Proton-sensing GPCRs are activated by released protons and essential for pH homeostasis (32, 33). The proton-sensing GPCR *Gpr68* is expressed in ameloblasts and the papillary layer of rat incisors, and *Gpr68*-KO mice were shown to have a hypomaturation type of enamel hypoplasia (34). It is possible that the regulatory mechanism of *Gpr115* is related to proton-sensing GPCRs that sense the pH of enamel amelo-

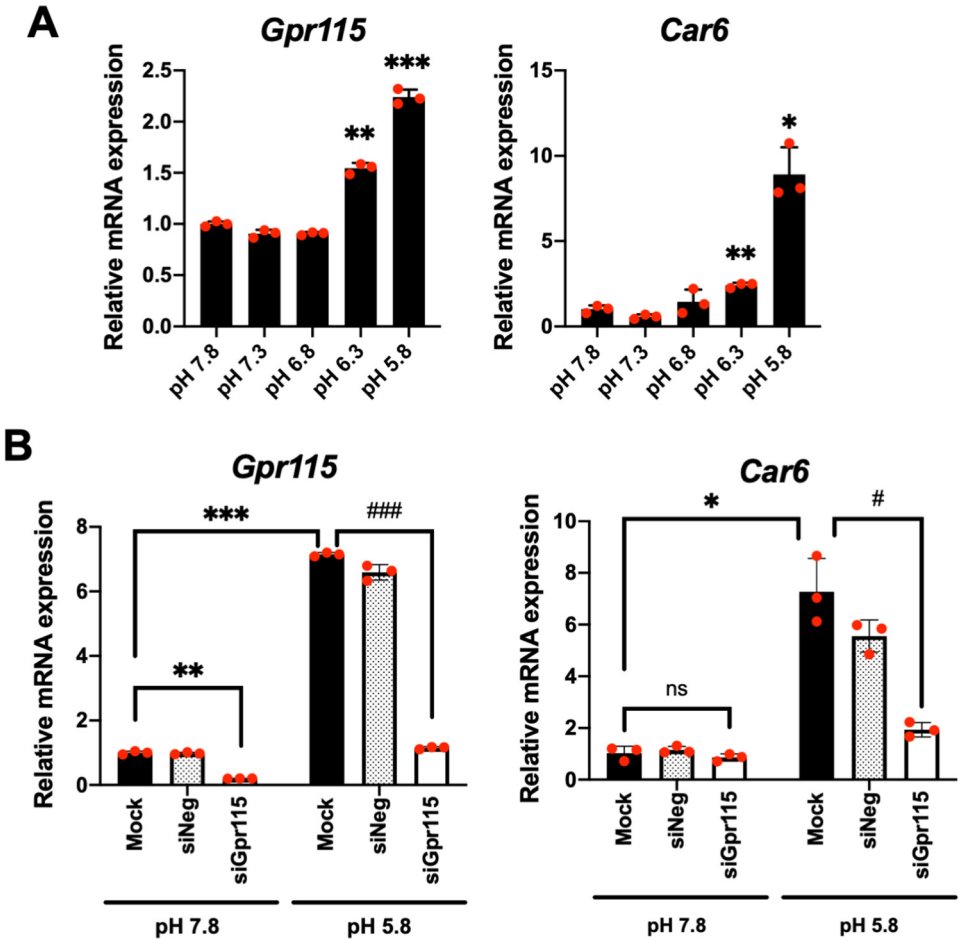

Figure 9. pH decline induced Car6 expression via Gpr115 in CLDE cells. *A*, mRNA expressions of *Gpr115* and *Car6* in CLDE cells cultured in media with different pH levels ($n = 3$). Mean values are shown as *bars*. *Error bars* represent S.D.; *, $p < 0.05$; **, $p < 0.01$; ***, $p < 0.001$; two-tailed *t* test. Three independent experiments were performed. *B*, mRNA expressions of *Gpr115* and *Car6* were determined in control mock without siRNA, and siNeg- and siGpr115-transfected CLDE cells cultured in media with different pH levels ($n = 3$). Mean values are shown as *bars*. *Error bars* represent S.D.; *ns*, $p > 0.05$; *, $p < 0.05$; **, $p < 0.01$; ***, $p < 0.001$ as compared with mock in pH 7.8 medium; two-tailed *t* test; #, $p < 0.05$; ###, $p < 0.001$ as compared with mock in pH 5.8 medium; two-tailed *t* test. Three independent experiments were performed.

blasts. Additional investigations to determine how ameloblasts detect protons in regard to tooth development are necessary. In the present study, the effects of pH decline on mineralization activity in CLDE cells was tested. However, mineralization did not occur at pH 5.8, as it was inhibited by that acidic condition (data not shown). Therefore it will be essential to establish an effective *in vitro* culture system to demonstrate how ameloblasts modulate pH during the enamel formation process.

Although *Gpr115* is preferentially expressed in developing skin, its loss in mice did not result in an overt phenotype in skin (35). In agreement with that report, the present *Gpr115*-KO mice were generated under a fetal condition and also demonstrated no obvious phenotype in skin. Another report suggested that expression of *Gpr115* occurs in the most apical layer of the epidermis (36). Different from enamel, epidermal tissue has a dynamic metabolic turnover, which may explain why the present *Gpr115*-KO mice develop normally in ectodermal tissues except in dental enamel. Prömel and colleagues (13, 35) suggested a biological redundancy of *Gpr115* with *Gpr111* (also known as adhesion G protein–coupled receptors subfamily F2, *Adgrf2*) that occurs in tandem with *Gpr115*. The expression of *Gpr111* during tooth development was not examined in the present experiments, although this might explain why deletion of *Gpr115* did not result in complete inhibition of enamel mineralization.

In summary, the present results identified a novel mechanism for regulation of pH by *Gpr115* during tooth development. Both *in vivo* and *in vitro* evidence suggests that *Gpr115* is expressed in ameloblasts during the maturation stage and induces *Car6* expression. As a result, ameloblasts gain a capacity to buffer pH for enamel mineralization. Taken together, these findings establish the essential role of *Gpr115* in tooth development and are the first to present detailed characterization of its biological function. These novel insights also provide important information regarding the activities of GPCRs in ectodermal organogenesis.

Experimental procedures

Generation of Gpr115-KO mice

The *Gpr115* targeting vector was designed by KOMP Repository Collection (CSD45717, Adgrf4$^{tm1a(KOMP)Wtsi}$) and injected into embryonic stem cells with the targeting strategy shown in Fig. 2*A*. Briefly, 5329 base pairs (bp) of the 5′ arm and 3374 bp

of the 3′ arm were recombined into the *Gpr115* locus, and loxP sites were recombined with exon 4 of *Gpr115*. For Cre-loxP recombination, CMV promoter–driven Cre mice were mated with *Gpr115*-floxed mice to generate *Gpr115*-null mice. Deletion of exon 4 results in a termination codon in seven different amino acids. Three generated mouse lines showed a similar tooth phenotype. The *Gpr115*-KO mouse line was maintained by crossmating with FVB/N mice. The animal protocol used in the present study was approved by the NIDCR Animal Care and Use Committee (protocol number ASP16-796). All animals were housed in a facility approved by the American Association for the Accreditation of Laboratory Animal Care.

Cell culture and transfection

The mouse cervical loop–derived dental epithelial cell line CLDE was maintained in keratinocyte serum-free medium supplemented with EGF and BPE (Invitrogen) at 37°C with 5% CO_2, as described previously (37). In a pH stimulation assay, 1 M HCl solution was added into culture medium to adjust pH. For RT-qPCR and mineralization assay examinations, CLDE cells were cultured until 80% confluency and transfected with Trilencer-27 Universal scrambled negative control siRNA duplex (OriGene, siNeg), *Adgrf4* Mouse siRNA Oligo Duplex (OriGene, siGpr115), and *Car6* Mouse siRNA Oligo Duplex (OriGene, siCar6) using Lipofectamine® RNAiMax Reagent (Invitrogen), following the manufacturer's protocol. For experiments with Car6 overexpression, a pCMV6-Entry Mammalian Expression Vector (OriGene, pCMV6) and mouse Car6 expression plasmid (OriGene, Car6) were transfected into CLDE cells using Lipofectamine® LTX with Plus Reagent (Invitrogen), following the manufacturer's protocol.

Northern blotting

Total RNA was extracted from P1 rat tissues using TRIzol reagent (Invitrogen), and 20 μg of RNA was separated by electrophoresis and transferred to a Nytran membrane (Schleicher & Schuell), as described previously (19). cDNA was labeled with [α-^{32}P]dCTP using Ready-To-Go DNA labeling beads (Amersham Biosciences). The membranes were incubated with labeled probes at 68°C in QuikHyb (Stratagene) and exposed to autoradiography film (Kodak).

RT-PCR and real-time PCR

Total RNA from mouse tooth germs as well as CLDE cells was isolated using an RNeasy Mini Kit (Qiagen), according to the manufacturer's protocol. cDNA was synthesized from 500 ng of total RNA using SuperScript™ VILO™ Master Mix (Invitrogen). Real-time PCR was performed using SYBR™ Select Master Mix (Invitrogen) with a Step One Plus™ Real-Time PCR System (Thermo Fisher Scientific). Relative mRNA expression was determined with GAPDH used as the internal control. The primer sequence used in this study were shown in Table 1.

Histological analysis, in situ hybridization, and immunofluorescence staining analysis

In situ hybridization was performed with frozen sections of P1 mouse heads, as described previously (38). Digoxigenin-11 UTP-labeled single-strand RNA probes for *Gpr115* sense and antisense strands were prepared using a digoxigenin RNA labeling kit (Roche Diagnostics). H-E and immunofluorescence staining were performed using paraffin-embedded tissues dissected and processed as described previously (21). For immunostaining, antigen retrieval was performed with citrate buffer (Sigma) and the sections underwent Power Block (BioGenex) application for 20 min prior to incubation with the primary antibody. The primary antibodies of GPR115 (Novus Biologicals, 1:200), CAR6 (US Biological, 1:100), and AMBN (Santa Cruz Biotechnology, 1:200) were used to detect proteins. Primary antibodies were detected using an Alexa Fluor 488 conjugated antibody (Invitrogen, 1:400). Nuclear staining was performed with DAPI (Sigma). Images were captured using FLUOVIEW FV10i confocal microscopy (Olympus).

Domain analysis of GPR115

The predicted protein sequence of GPR115 was obtained from NCBI GenBank (http://www.ncbi.nlm.nih.gov/genbank/) and analyzed using PROSITE (39).

micro-CT analysis

Heads from 8-week-old mice were dissected and fixed with 4% paraformaldehyde in PBS. Scanning was performed using a SCANCO μCT50 device, as described previously (17). 3D reconstruction and enamel and dentin volume quantification were conducted using AnalyzePro (AnalyzeDirect).

SEM and SEM-EDX analysis

Incisors of 8-week-old mice were extracted and embedded using an EMbed 812 Kit (Electron Microscopy Science), then sectioned in the middle frontal area. Sectioned layers were etched with 0.1% nitric acid three times for 10 s each and with 10% sodium hypochlorite for 15 s. After etching, 5 nm sputter coating with gold-palladium was performed. The samples were scanned using a Miniscope® TM3000 (Hitachi).

pH indicator staining

Bromphenol red staining and resazurin were used to indicate pH levels of enamel, as described previously (26, 31, 40–42). Bromphenol red at 100 mg was dissolved in 45 ml of distilled water containing 0.1% ethanol. Resazurin at 100 mg was dissolved in 45 ml of distilled water. Mandibular incisors were dissected from mouse mandibles, then after removal of soft tissue were dipped into staining solution for 1 min and washed with 100% ethanol and water. Images were acquired using a Leica S8AP0 microscope (Leica). The length of the stained portion of the incisor was calculated as percentage of total incisor length.

RNA-Seq

To construct each cDNA library, total RNA in P7 first molars from littermate WT and Gpr115-KO mice was extracted using TRIzol reagent (Invitrogen). cDNA libraries were produced using a Nextera XT library kit (Illumina), and samples were run on a HiSeq1500 (Illumina) configured for 150 × 150 pair-end reads. Differential gene expression analysis was performed with

ASBMB

Table 1
Primer sequences used in this study

Primer	Forward	Reverse	Product size
Primers for RT-PCR/RT-qPCR			
mGpr115 (exon 4)	GCTGTCCTTGGAACTTCCGT	GTCCACAGAGAGACTTGTGCA	95
mAmbn	TCCGAAAACCCACCAACACCTG	AGCGGATGCTTTGTTGTGTGCC	123
mDspp	AACTCTGTGGCTGTGCCTCT	TATTGACTCGGAGCCATTCC	171
mrGapdh	GGTGAAGGTCGGTGTGAACG	CTCGCTCCTGGAAGATGGTG	233
mEnam	TGCAGAAAGCCCAAACCCAAGT	TTTGGCTGAGAAGAGCTGGCTT	132
mrMmp-20	GGCGAGATGGTGGCAAGAG	CTGGGAAGAGGCGGTAGTT	166
mAmtn	GACCTGCCGTTGTTCAACCC	TGGGTAACATCTGCGGTTGC	109
mKlk4	TTGCAAACGATCTCATGCTC	TGAGGTGGTACACAGGGTCA	228
mAlpl	TGTGGAATACGAACTGGATGAG	AGTGGGAATGCTTGTGTCTG	104
Primers for genotyping			
Gpr115-genotyping	AAACTTGGCCTTGGAATGGTGATGG	GACTTCACCGTGATTGCCTATGTGG	1756/916

DESeq2 (43). For GO analysis, online platform for GO Enrichment Analysis provided by the Gene Ontology Consortium (http://geneontology.org) was used (44, 45).

Mineralization assay

CLDE cells were cultured in 12-well plates, then after transfection of siRNAs were cultured in DMEM/F12 (Invitrogen) with 2.5 mM of calcium chloride (MP Biomedicals), 10 mM of β-glycerophosphate (Sigma), 50 μM of L-ascorbic acid (Sigma), and 10 μM of calcitriol (TCI Chemicals) for 2 or 4 weeks. After washing with PBS, cells were fixed with 4% paraformaldehyde in PBS for 5 min. For Alizarin Red staining, cells were rinsed with water and stained with freshly made 1% Alizarin Red S solution (Sigma) for 10 min, as described previously (46). Staining was stopped using 400 μl of 1% SDS for 15 min and absorbance of the 450 nm wavelength was measured using a TriStar^2 LB 942 (Berthold).

Statistics

A two-tailed Student's *t* test was applied for statistical analysis of two independent variables. *P* values <0.05 were considered to indicate statistical significance. GraphPad Prism 8 was used for all statistical analyses.

Data availability

The RNA-Seq data presented in this paper have all been deposited with the NCBI GEO GSE155641. All remaining data are contained within the article.

Acknowledgments—This work is dedicated to the memory of Dr. Yoshihiko Yamada, who passed away in 2019. He was a pioneer in matrix biology, and a mentor and friend to many. We thank Dr. Olivier Duverger and Dr. Emily Y. Chu for their kind technical advice. We also thank Dr. Ashok Kulkarni, Glenn Longnecker, and the NIDCR Gene Targeting Core Facility for performing the embryonic stem cell injections to generate *Gpr115*-KO mice. This work utilized the computational resources of the National Institutes of Health HPC Biowulf cluster (http://hpc.nih.gov). The NIDCD/Genomics and Computational Biology Core, National Institutes of Health Grant ZIC DC000086 (to the GCBC).

Author contributions—Y. C., K. Y., K. S., T. Ikeuchi, T. Iwamoto, T. N., S. d. V., E. T. B., and D. M. data curation; Y. C. formal analysis; Y. C., K. Y., K. S., T. Ikeuchi, T. Iwamoto, T. N., S. d. V., E. T. B., and D. M. investigation; Y. C. visualization; Y. C. writing-original draft; K. Y., K. S., T. Ikeuchi, T. Iwamoto, C. R., R. J. M., H. I., and C. K. B. supervision; K. Y., K. S., C. R., Y. Y., and S. F. writing-review and editing; R. J. M. and C. K. B. methodology; R. H., A. Y., Y. Y., and S. F. funding acquisition; Y. Y. and S. F. conceptualization; Y. Y. and S. F. project administration.

Funding and additional information—This work was supported in part by the Intramural Research Program of NIDCR, National Institutes of Health, Grant 1ZIADE000720-11 (to Y. Y.), the NIDCR Transfer Core Facility, National Institutes of Health, Grant ZIC DE000744-04 (to Y. Y.). Grant-in-Aid support was also received from the Japan Society for the Promotion of Science (JSPS) KAKENHI 17H01606 (to S. F.), 18H06286 to (to Y. C.), 18H03009 (to K. S.), 18K19634 (to T. N.). The content is solely the responsibility of the authors and does not necessarily represent the official views of the National Institutes of Health.

Conflict of interest—The authors declare that they have no conflicts of interest with the contents of this article.

Abbreviations—The abbreviations used are: IEE, inner enamel epithelium; AMBN, ameloblastin; GPCR, G protein–coupled receptor; CLDE, cervical loop–derived dental epithelial cell line; P, postnatal day; SEM, scanning electron microscopy; EDX, energy-dispersive X-ray spectroscopy; GO, gene ontology; CMV, cytomegalovirus; aa, amino acid.

References

1. Lacruz, R. S., Habelitz, S., Wright, J. T., and Paine, M. L. (2017) Dental enamel formation and implications for oral health and disease. *Physiol. Rev.* **97,** 939–993 CrossRef Medline
2. Thesleff, I. (2003) Epithelial-mesenchymal signalling regulating tooth morphogenesis. *J. Cell Sci.* **116,** 1647–1648 CrossRef Medline
3. Li, C. Y., Cha, W., Luder, H. U., Charles, R. P., McMahon, M., Mitsiadis, T. A., and Klein, O. D. (2012) E-cadherin regulates the behavior and fate of epithelial stem cells and their progeny in the mouse incisor. *Dev. Biol.* **366,** 357–366 CrossRef Medline
4. Fukumoto, S., Yamada, A., Nonaka, K., and Yamada, Y. (2005) Essential roles of ameloblastin in maintaining ameloblast differentiation and enamel formation. *Cells Tissues Organs* **181,** 189–195 CrossRef Medline
5. Aurrekoetxea, M., Irastorza, I., Garcia-Gallastegui, P., Jimenez-Rojo, L., Nakamura, T., Yamada, Y., Ibarretxe, G., and Unda, F. J. (2016) Wnt/β-catenin regulates the activity of epiprofin/Sp6, SHH, FGF, and BMP to coordinate the stages of odontogenesis. *Front. Cell Dev. Biol.* **4,** 25 CrossRef Medline

6. Ibarretxe, G., Aurrekoetxea, M., Crende, O., Badiola, I., Jimenez-Rojo, L., Nakamura, T., Yamada, Y., and Unda, F. (2012) Epiprofin/Sp6 regulates Wnt-BMP signaling and the establishment of cellular junctions during the bell stage of tooth development. *Cell Tissue Res.* **350,** 95–107 CrossRef Medline
7. Smith, C. E. (1998) Cellular and chemical events during enamel maturation. *Crit. Rev. Oral Biol. Med.* **9,** 128–161 CrossRef Medline
8. Bronckers, A. L. (2017) Ion transport by ameloblasts during amelogenesis. *J. Dent. Res.* **96,** 243–253 CrossRef Medline
9. Duan, X. (2014) Ion channels, channelopathies, and tooth formation. *J. Dent. Res.* **93,** 117–125 CrossRef Medline
10. Lacruz, R. S., Smith, C. E., Kurtz, I., Hubbard, M. J., and Paine, M. L. (2013) New paradigms on the transport functions of maturation-stage ameloblasts. *J. Dent. Res.* **92,** 122–129 CrossRef Medline
11. Simmer, J. P., and Fincham, A. G. (1995) Molecular mechanisms of dental enamel formation. *Crit. Rev. Oral Biol. Med.* **6,** 84–108 CrossRef Medline
12. Damkier, H. H., Josephsen, K., Takano, Y., Zahn, D., Fejerskov, O., and Frische, S. (2014) Fluctuations in surface pH of maturing rat incisor enamel are a result of cycles of H^+-secretion by ameloblasts and variations in enamel buffer characteristics. *Bone* **60,** 227–234 CrossRef Medline
13. Hamann, J., Aust, G., Araç, D., Engel, F. B., Formstone, C., Fredriksson, R., Hall, R. A., Harty, B. L., Kirchhoff, C., Knapp, B., Krishnan, A., Liebscher, I., Lin, H. H., Martinelli, D. C., Monk, K. R., *et al.* (2015) International Union of Basic and Clinical Pharmacology. XCIV. Adhesion G protein-coupled receptors. *Pharmacol. Rev.* **67,** 338–367 CrossRef Medline
14. Regard, J. B., Sato, I. T., and Coughlin, S. R. (2008) Anatomical profiling of G protein-coupled receptor expression. *Cell* **135,** 561–571 CrossRef Medline
15. Patra, C., van Amerongen, M. J., Ghosh, S., Ricciardi, F., Sajjad, A., Novoyatleva, T., Mogha, A., Monk, K. R., Mühlfeld, C., and Engel, F. B. (2013) Organ-specific function of adhesion G protein-coupled receptor GPR126 is domain-dependent. *Proc. Natl. Acad. Sci. U. S. A.* **110,** 16898–16903 CrossRef Medline
16. Nakamura, T., Unda, F., de Vega, S., Vilaxa, A., Fukumoto, S., Yamada, K. M., and Yamada, Y. (2004) The Krüppel-like factor epiprofin is expressed by epithelium of developing teeth, hair follicles, and limb buds and promotes cell proliferation. *J. Biol. Chem.* **279,** 626–634 CrossRef Medline
17. Chiba, Y., He, B., Yoshizaki, K., Rhodes, C., Ishijima, M., Bleck, C. K. E., Stempinski, E., Chu, E. Y., Nakamura, T., Iwamoto, T., de Vega, S., Saito, K., Fukumoto, S., and Yamada, Y. (2019) The transcription factor AmeloD stimulates epithelial cell motility essential for tooth morphology. *J. Biol. Chem.* **294,** 3406–3418 CrossRef Medline
18. Nakamura, T., de Vega, S., Fukumoto, S., Jimenez, L., Unda, F., and Yamada, Y. (2008) Transcription factor epiprofin is essential for tooth morphogenesis by regulating epithelial cell fate and tooth number. *J. Biol. Chem.* **283,** 4825–4833 CrossRef Medline
19. Iwamoto, T., Nakamura, T., Ishikawa, M., Yoshizaki, K., Sugimoto, A., Ida-Yonemochi, H., Ohshima, H., Saito, M., Yamada, Y., and Fukumoto, S. (2017) Pannexin 3 regulates proliferation and differentiation of odontoblasts via its hemichannel activities. *PLoS One* **12,** e0177557 CrossRef Medline
20. Miyazaki, K., Yoshizaki, K., Arai, C., Yamada, A., Saito, K., Ishikawa, M., Xue, H., Funada, K., Haruyama, N., Yamada, Y., Fukumoto, S., and Takahashi, I. (2016) Plakophilin-1, a novel Wnt signaling regulator, is critical for tooth development and ameloblast differentiation. *PLoS One* **11,** e0152206 CrossRef Medline
21. Nakamura, T., Chiba, Y., Naruse, M., Saito, K., Harada, H., and Fukumoto, S. (2016) Globoside accelerates the differentiation of dental epithelial cells into ameloblasts. *Int. J. Oral Sci.* **8,** 205–212 CrossRef Medline
22. Liu, J., Saito, K., Maruya, Y., Nakamura, T., Yamada, A., Fukumoto, E., Ishikawa, M., Iwamoto, T., Miyazaki, K., Yoshizaki, K., Ge, L., and Fukumoto, S. (2016) Mutant GDF5 enhances ameloblast differentiation via accelerated BMP2-induced Smad1/5/8 phosphorylation. *Sci. Rep.* **6,** 23670–23670 CrossRef Medline
23. Arai, C., Yoshizaki, K., Miyazaki, K., Saito, K., Yamada, A., Han, X., Funada, K., Fukumoto, E., Haruyama, N., Iwamoto, T., Takahashi, I., and Fukumoto, S. (2017) Nephronectin plays critical roles in Sox2 expression and proliferation in dental epithelial stem cells via EGF-like repeat domains. *Sci. Rep.* **7,** 45181–45181 CrossRef Medline
24. Han, X., Yoshizaki, K., Miyazaki, K., Arai, C., Funada, K., Yuta, T., Tian, T., Chiba, Y., Saito, K., Iwamoto, T., Yamada, A., Takahashi, I., and Fukumoto, S. (2018) The transcription factor NKX2-3 mediates p21 expression and ectodysplasin-A signaling in the enamel knot for cusp formation in tooth development. *J. Biol. Chem.* **293,** 14572–14584 CrossRef Medline
25. Saito, Y., Kaneda, K., Suekane, A., Ichihara, E., Nakahata, S., Yamakawa, N., Nagai, K., Mizuno, N., Kogawa, K., Miura, I., Itoh, H., and Morishita, K. (2013) Maintenance of the hematopoietic stem cell pool in bone marrow niches by EVI1-regulated GPR56. *Leukemia* **27,** 1637–1649 CrossRef Medline
26. Bronckers, A. L., Lyaruu, D. M., Guo, J., Bijvelds, M. J., Bervoets, T. J., Zandieh-Doulabi, B., Medina, J. F., Li, Z., Zhang, Y., and DenBesten, P. K. (2015) Composition of mineralizing incisor enamel in cystic fibrosis transmembrane conductance regulator-deficient mice. *Eur. J. Oral Sci.* **123,** 9–16 CrossRef Medline
27. Wen, X., and Paine, M. L. (2013) Iron deposition and ferritin heavy chain (Fth) localization in rodent teeth. *BMC Res Notes* **6,** 1 CrossRef Medline
28. Bori, E., Guo, J., Rácz, R., Burghardt, B., Földes, A., Kerémi, B., Harada, H., Steward, M. C., Den Besten, P., Bronckers, A. L., and Varga, G. (2016) Evidence for bicarbonate secretion by ameloblasts in a novel cellular model. *J. Dent. Res.* **95,** 588–596 CrossRef Medline
29. Reibring, C. G., El Shahawy, M., Hallberg, K., Kannius-Janson, M., Nilsson, J., Parkkila, S., Sly, W. S., Waheed, A., Linde, A., and Gritli-Linde, A. (2014) Expression patterns and subcellular localization of carbonic anhydrases are developmentally regulated during tooth formation. *PLoS One* **9,** e96007 CrossRef Medline
30. Lacruz, R. S., Hilvo, M., Kurtz, I., and Paine, M. L. (2010) A survey of carbonic anhydrase mRNA expression in enamel cells. *Biochem. Biophys. Res. Commun.* **393,** 883–887 CrossRef Medline
31. Duverger, O., Ohara, T., Bible, P. W., Zah, A., and Morasso, M. I. (2017) DLX3-dependent regulation of ion transporters and carbonic anhydrases is crucial for enamel mineralization. *J. Bone Miner. Res.* **32,** 641–653 CrossRef Medline
32. Ludwig, M. G., Vanek, M., Guerini, D., Gasser, J. A., Jones, C. E., Junker, U., Hofstetter, H., Wolf, R. M., and Seuwen, K. (2003) Proton-sensing G-protein-coupled receptors. *Nature* **425,** 93–98 CrossRef Medline
33. Li, H., Wang, D., Singh, L. S., Berk, M., Tan, H., Zhao, Z., Steinmetz, R., Kirmani, K., Wei, G., and Xu, Y. (2009) Abnormalities in osteoclastogenesis and decreased tumorigenesis in mice deficient for ovarian cancer G protein-coupled receptor 1. *PLoS One* **4,** e5705 CrossRef Medline
34. Parry, D. A., Smith, C. E., El-Sayed, W., Poulter, J. A., Shore, R. C., Logan, C. V., Mogi, C., Sato, K., Okajima, F., Harada, A., Zhang, H., Koruyucu, M., Seymen, F., Hu, J. C., Simmer, J. P., *et al.* (2016) Mutations in the pH-sensing G-protein-coupled receptor GPR68 cause amelogenesis imperfecta. *Am. J. Hum. Genet.* **99,** 984–990 CrossRef Medline
35. Prömel, S., Waller-Evans, H., Dixon, J., Zahn, D., Colledge, W. H., Doran, J., Carlton, M. B., Grosse, J., Schöneberg, T., Russ, A. P., and Langenhan, T. (2012) Characterization and functional study of a cluster of four highly conserved orphan adhesion-GPCR in mouse. *Dev. Dyn.* **241,** 1591–1602 CrossRef Medline
36. Gerber, P. A., Hevezi, P., Buhren, B. A., Martinez, C., Schrumpf, H., Gasis, M., Grether-Beck, S., Krutmann, J., Homey, B., and Zlotnik, A. (2013) Systematic identification and characterization of novel human skin-associated genes encoding membrane and secreted proteins. *PLoS One* **8,** e63949 CrossRef Medline
37. Yoshizaki, K., Hu, L., Nguyen, T., Sakai, K., He, B., Fong, C., Yamada, Y., Bikle, D. D., and Oda, Y. (2014) Ablation of coactivator Med1 switches the cell fate of dental epithelia to that generating hair. *PLoS One* **9,** e99991 CrossRef Medline
38. He, B., Chiba, Y., Li, H., de Vega, S., Tanaka, K., Yoshizaki, K., Ishijima, M., Yuasa, K., Ishikawa, M., Rhodes, C., Sakai, K., Zhang, P., Fukumoto, S., Zhou, X., and Yamada, Y. (2019) Identification of the novel tooth-specific transcription factor AmeloD. *J. Dent. Res.* **98,** 234–241 CrossRef Medline
39. de Castro, E., Sigrist, C. J., Gattiker, A., Bulliard, V., Langendijk-Genevaux, P. S., Gasteiger, E., Bairoch, A., and Hulo, N. (2006) ScanProsite: Detection of PROSITE signature matches and ProRule-associated functional and structural residues in proteins. *Nucleic Acids Res.* **34,** W362–W365 CrossRef Medline

ASBMB

40. Tye, C. E., Sharma, R., Smith, C. E., and Bartlett, J. D. (2010) Altered ion-responsive gene expression in Mmp20 null mice. *J. Dent. Res.* **89,** 1421–1426 CrossRef Medline
41. Sasaki, S., Takagi, T., and Suzuki, M. (1991) Cyclical changes in pH in bovine developing enamel as sequential bands. *Arch. Oral Biol.* **36,** 227–231 CrossRef Medline
42. Wang, S. K., Hu, Y., Yang, J., Smith, C. E., Nunez, S. M., Richardson, A. S., Pal, S., Samann, A. C., Hu, J. C., and Simmer, J. P. (2015) Critical roles for WDR72 in calcium transport and matrix protein removal during enamel maturation. *Mol. Genet. Genomic Med.* **3,** 302–319 CrossRef Medline
43. Love, M. I., Huber, W., and Anders, S. (2014) Moderated estimation of fold change and dispersion for RNA-Seq data with DESeq2. *Genome Biol.* **15,** 550 CrossRef Medline
44. Ashburner, M., Ball, C. A., Blake, J. A., Botstein, D., Butler, H., Cherry, J. M., Davis, A. P., Dolinski, K., Dwight, S. S., Eppig, J. T., Harris, M. A., Hill, D. P., Issel-Tarver, L., Kasarskis, A., Lewis, S., *et al.* (2000) Gene ontology: Tool for the unification of biology. The Gene Ontology Consortium. *Nat. Genet.* **25,** 25–29 CrossRef Medline
45. Mi, H., Muruganujan, A., Ebert, D., Huang, X., and Thomas, P. D. (2019) PANTHER version 14: More genomes, a new PANTHER GO-slim and improvements in enrichment analysis tools. *Nucleic Acids Res.* **47,** D419–D426 CrossRef Medline
46. Nakamura, T., Naruse, M., Chiba, Y., Komori, T., Sasaki, K., Iwamoto, M., and Fukumoto, S. (2015) Novel hedgehog agonists promote osteoblast differentiation in mesenchymal stem cells. *J. Cell. Physiol.* **230,** 922–929 CrossRef Medline